Palaeogeography, Palaeoclimatology, Palaeoecology 459 (2016) 488–494

Contents lists available at ScienceDirect

Palaeogeography, Palaeoclimatology, Palaeoecology

journal homepage: www.elsevier.com/locate/palaeo

Provenance of Neogene eolian red clay in the Altun region of western China—Insights from U—Pb detrital zircon age data

Feng Pan [a], Jianxing Li [a,*], Yong Xu [a], Leping Yue [b], Michael T.D. Wingate [c], Yanguang Li [a], Lin Guo [a], Rengang Xi [a], Lei Guo [a]

[a] Research Center for Orogenic Geology, Xi'an Center of Geological Survey, Geological Survey of China, Xi'an, PR China
[b] State Key Laboratory for Continental Dynamics, Department of Geology, Northwest University, Xi'an, PR China
[c] Geological Survey of Western Australia, East Perth, Western Australia, Australia

ARTICLE INFO

Article history:
Received 24 February 2016
Received in revised form 1 July 2016
Accepted 18 July 2016
Available online 19 July 2016

Keywords:
Red clay
Detrital zircon
Provenance
Neogene
Eolian deposits

ABSTRACT

Aridity of the Asian interior plays an important role in the accumulation of eolian deposits in both eastern (monsoon regime) and western China (westerly wind regime). A better understanding of the provenance of those eolian deposits (loess and red clay) will shed light on the history and mechanisms of Asian aridification. In eastern China, decrease in grain size from northwest to southeast shows that the Neogene red clay of the Chinese Loess Plateau (CLP) was derived from the desert and arid lands of northwestern China by the East Asian winter monsoon. However, in western China, outcrops are limited, and this is an obstacle to studies of the spatial variation of the provenance of eolian deposits. We use U—Pb geochronology of detrital zircons to determine the provenance of the Altun Red Clay, a recently discovered and continuous eolian deposit in western China. Our comparison of detrital zircon age spectra for the Altun Red Clay with those of potential source regions, and with results for the coeval red clay of the CLP, indicates that: 1. the main zircon age components of the Altun Red Clay are very different from those of the red clay on the CLP, suggesting that these deposits were sourced from different areas, and 2. the Altun Red Clay was likely sourced from the Taklamakan Desert, and transported via westerly winds.

1. Introduction

Within the larger scheme of Cenozoic aridification of the Asian interior, east-central China is dominated by northwesterly and southeasterly monsoon winds, whereas western China is dominated by a westerly wind regime (Fig. 1a; An et al., 2000; Guo et al., 2002; Li et al., 2014; Qiang et al., 2011; Sun et al., 2010, Sun and Windley, 2015; Xu et al., 2009; Yue, 1995). Studies of the provenance and transporting wind patterns of the typical eolian deposits of loess and red clay have provided a basis for reconstructing Neogene–Quaternary sediment transport pathways and paleogeography.

Most progress has been made by numerous studies in the monsoon-dominated area of east-central China due to the depth, continuity, and large areal extent of the loess and red clay deposits on the Chinese Loess Plateau (CLP) (Che and Li, 2013; Nie et al., 2014, 2015; Pullen et al., 2011; Shang et al., 2016; Stevens et al., 2013; Xiao et al., 2012). Studies of the microstructural surface features of quartz grains (Lu et al., 1976), geochemical and mineral tracers, and Nd and Sr isotopes (Chen et al., 2007; Jahn et al., 2001; Li et al., 2009; Sun et al., 2008), have been widely used to trace the provenance of eolian dust on the CLP. The grain size of Quaternary loess and Neogene red clay on the CLP also decreases gradually from north to south, indicating that the desert and arid lands of northwestern China (Fig. 1a) are the major eolian provenance areas and that dust was transported mainly by the northerly winter monsoon (Lu et al., 2001; Miao et al., 2004; Sun et al., 2010). The Alxa arid lands are still a center of modern dust storm activity in northern China (Sun et al., 2001; Wang et al., 2004). Furthermore, recent studies have led to a new conceptual model associating loess on the CLP with the development of the Yellow River system during the Pliocene and Pleistocene (Stevens et al., 2013; Nie et al., 2015).

Fewer studies have been undertaken in western China (Fig. 1a), where limited Neogene red clay sequences have been explored in the Junggar Basin (Sun et al., 2010) and in the Altun Shan (Li et al., 2014). Pronounced differences in Sr and Nd isotope compositions of eolian deposits in the Junggar Basin and the CLP imply that the two deposits had different sources, and that the Junggar Basin deposits were probably transported from Kazakhstan in the west (Sun et al., 2010). However, there have been no provenance studies of the Altun Red Clay, which might have had sources different from those of the Junggar Basin deposits, particularly given the large distance (c. 700 km) between the two areas and their different ages of deposition.

U—Pb geochronology of detrital zircons provides a new opportunity to determine the source of eolian deposits (Nie et al., 2014; Pullen et al.,

* Corresponding author.
E-mail address: ljianxing2005@163.com (J. Li).

http://dx.doi.org/10.1016/j.palaeo.2016.07.020
0031-0182/

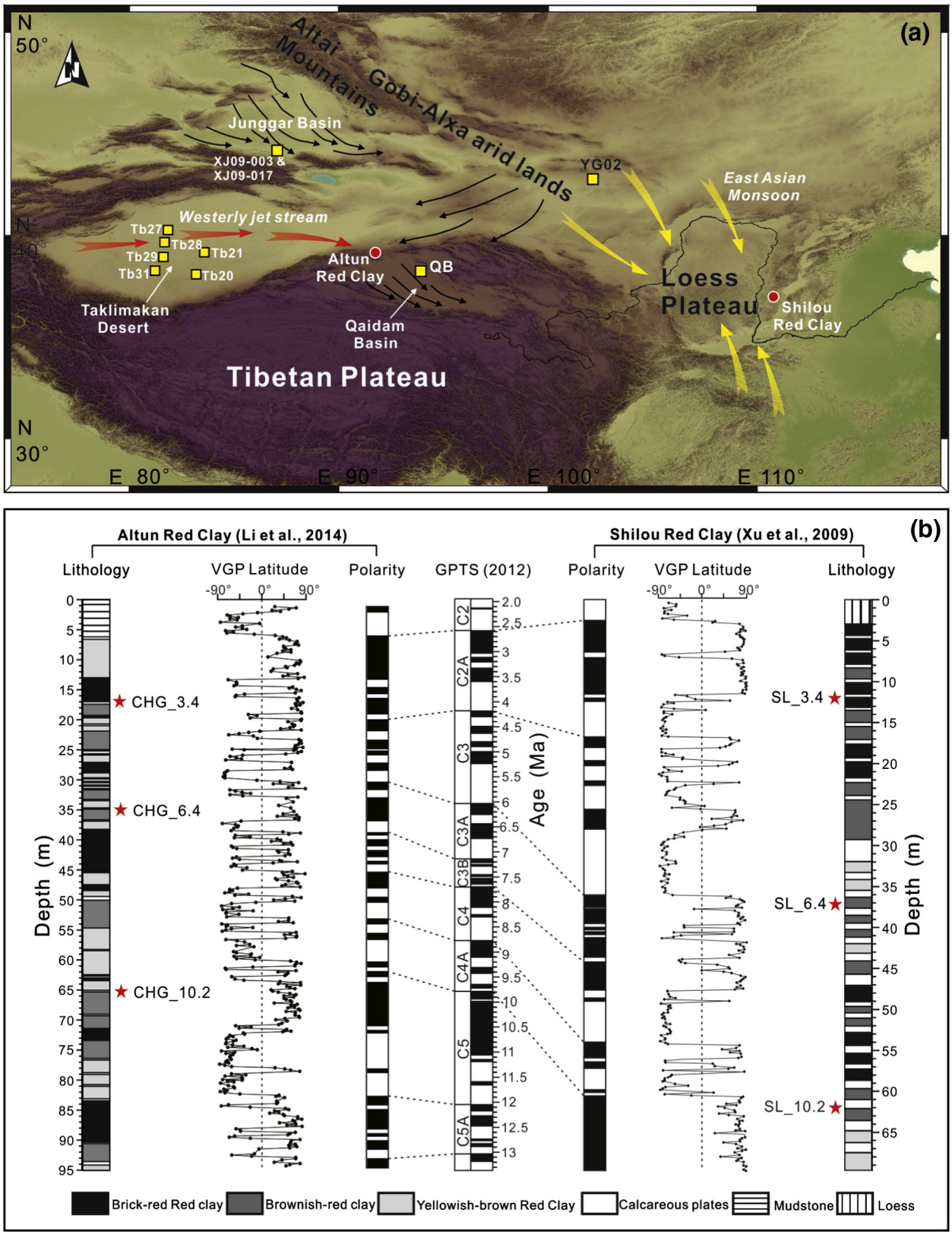

Fig. 1. (a) Map showing the present major wind system in northern China, and the locations (circles) of the Altun Red Clay in the northern Tibetan Plateau, and the Shilou Red Clay on the Chinese Loess Plateau. Squares indicate the locations of potential source area samples with published zircon ages: dune samples from the central sand sea of the Taklamakan Desert (Tb20, 21, 27, 28, 29, 31, Rittner et al., 2016); fluvial sediments from the Gobi–Alxa arid lands (YG02, Che and Li, 2013); fluvial-lacustrine sediments from the Qaidam Basin (QB, Pullen et al., 2011); and Neogene fluvial sediments from the Junggar Basin (XJ09-003 and XJ09-017, Yang et al., 2013). Black arrows show the prevailing near-surface winds; larger arrows show the pathways of the westerly jet stream and the East Asian monsoon. (b) Lithology and magnetostratigraphy of the Altun and Shilou Red Clay. Red stars indicate samples for U—Pb zircon dating. (For interpretation of the references to color in this figure legend, the reader is referred to the web version of this article.)

2011; Stevens et al., 2013; Újvári and Klötzli, 2015; Xiao et al., 2012). Recent studies have demonstrated that detrital zircon provenance analysis is more diagnostic than the average signal provided by bulk geochemistry in identifying the source areas of eolian deposits (Stevens et al., 2010; Újvári et al., 2013). The contrasting geological settings of the desert areas in northwestern China generate very different zircon ages, which could be used to discriminate between potential source areas of eolian deposits (Stevens et al., 2010).

In this contribution, we present new U—Pb detrital zircon age spectra for the Altun Red Clay, and also for the coeval Shilou Red Clay of the eastern CLP (Xu et al., 2009). We explore the similarities and differences in provenance and transport pattern between the western and eastern eolian red clay sequences and provide a better understanding of the monsoon and westerly wind regimes. We identify the source of the Altun Red Clay by comparing its age spectrum with published U—Pb zircon results from potential source areas. Because the detrital source(s) may have changed with time, and because of limited sample availability in both sequences, we sampled rocks of three different ages (10.2, 6.4, and 3.4 Ma, as determined previously by magnetostratigraphy; Li et al., 2014; Xu et al., 2009) in both the Altun and Shilou Red Clays.

2. Materials and methods

The Altun Red Clay sequence (Fig. 1a) is located at Caihonggou (CHG) in the eastern Xorhol Basin, northeast of the Tibetan Plateau, in the westerly wind regime area. Previous study has confirmed its eolian origin (Li et al., 2014). The eolian deposit, the main part of the CHG Formation, is 88.4 m thick, and contains 40 visually defined, brownish red clay and gray calcium nodule layers. According to the color and ration of red clay and calcium, the red clay sequence can be further divided into two parts: an upper part dominated by brownish-red clay with interbedded brownish-yellow calcareous plates (8:1–10:1), some of which pinch out along strike, and a lower part mainly composed of yellowish-brown clay with gray caliche nodule layers (4:1–5:1). Locally, there is water-lain, fine-grained sandstone and siltstone in the eolian deposit. Magnetostratigraphic and biostratigraphic results show that the Altun Red Clay was deposited between ~13 and 2.6 Ma (Li et al., 2014). This is the only continuous Neogene red clay sequence discovered so far in western China. Three samples for U—Pb zircon dating (CHG_10.2, CHG_6.4, CHG_3.4) were collected at depths of 65.2, 35.0, and 17.0 m within the CHG section, corresponding to depositional ages of 10.2, 6.4, and 3.4 Ma, respectively (Fig. 1b). The Shilou Red Clay (SL) sequence (Fig. 1a) is located at the eastern margin of the CLP, in the monsoon-dominated area. The Shilou red clay section is 72 m thick and contains 73 red clay and carbonate nodule couplets and ranges in age from 11 to 2.6 Ma (Xu et al., 2009). Three samples for U—Pb zircon dating (SL_10.2, SL_6.4, SL_3.4) were collected from depths of 61.9, 37.3, and 12.0 m, corresponding to depositional ages of 10.2, 6.4, and 3.4 Ma (Fig. 1b).

Detrital zircons from the six samples were separated by conventional high-density liquid and magnetic methods and selected randomly for analysis. Zircons were imaged using transmitted light and with cathodoluminescence (CL) techniques to characterize their internal structures and guide subsequent analysis. U—Pb zircon ages were determined by LA-ICPMS at the Key Laboratory for the Study of Focused Magmatism and Giant Ore Deposits, in the Xi'an Institute of Geology and Mineral Resources. The analyses employed a laser spot diameter of 32 μm (CHG_3.4, CHG_6.4, first-round CHG_10.2) and 24 μm (second-round CHG_10.2, SL_3.4, SL_6.4, SL_10.2). Laser-induced, depth- and time-dependent elemental fractionation and instrumental mass bias were corrected by reference to zircon standard 91,500 (Wiedenbeck et al., 2004) and glass standard NIST SRM610. U–Pb data were processed using GLITTER v. 4.4 (Van Achterbergh et al., 2001). The ages reported here are based on $^{238}U/^{206}Pb$ ratios for analyses younger than 1000 Ma and $^{207}Pb/^{206}Pb$ ratios for older analyses, and are not corrected for common lead. Analyses >10% discordant are rejected. All analytical results are tabulated in the Supplementary Data File.

To explore the provenance of Altun Red Clay, we compare our new results with published U—Pb zircon results from potential source areas. Eolian deposits, such as red clay, are taken to be products of the aridification of the Asian interior, because extensive deserts are needed as sources of dust for such deposits (Guo et al., 2001, 2002; Liu, 1985; Sun et al., 2010; Whalley et al., 1982). Therefore, inland basins and large desert areas are the most likely source areas for the eolian deposits. Taking into account likely climate and transport patterns in the past, the Qaidam and Junggar Basins, Taklamakan Desert, Gobi-Alxa arid lands, and other arid basins in western China are all potential sources of eolian dust (Chen et al., 2007; Derbyshire et al., 1998; Ding et al., 2001; Liu et al., 1994; Liu, 1985; Maher et al., 2009; Sun, 2002; Wu et al., 2010), and this has been demonstrated in previous detrital zircon studies (Che and Li, 2013; Pullen et al., 2011; Nie et al., 2014).

The detrital zircon age data are visualised and compared using combined probability density diagrams and histograms. We also employ a multidimensional scaling (MDS) statistical technique (Vermeesch, 2013), related to principle components analysis (PCA), to explore these large detrital zircon datasets. The MDS uses measures of difference to group samples with similar age spectra, and disperse samples with dissimilar ones. MDS can provide a visually effective way of comparing U—Pb zircon data and has been shown to differentiate effectively between sediments with different source characteristics (Stevens et al., 2013).

However, nearest neighbours in MDS plots and similarity of age spectra may be insufficient to draw robust conclusions about provenance because of the likelihood of mixing of eolian deposits from different sources. Similarities or neighbouring relationships in age spectra or MDS diagrams can be used to infer likely sources only if considered together with geological and climatic evidences and potential paleowind directions.

3. Results

The three Altun Red Clay (CHG) samples exhibit similar age spectra, with a dominant 560–400 Ma age component and a subordinate 400–200 Ma age component (Fig. 2a-c). In contrast, the three Shilou Red Clay (SL) samples from the eastern CLP exhibit a major 360–200 Ma age component, and relatively few analyses between 560 and 400 Ma. The three SL samples also show significant peaks of Paleoproterozoic age (Fig. 2h–j).

To constrain the sources of the Altun Red Clay, we compare its age spectra with published zircon age data from potential source areas (Fig. 2d–g), including: 1. dune samples from the central sand sea of the Taklamakan Desert (Tb20, 21, 27, 28, 29, 31) (Rittner et al., 2016); 2. fluvial sediment (YG02) from the Gobi–Alxa arid lands (Che and Li, 2013); 3. Plio-Pleistocene fluvial-lacustrine sediments (QB) from the Qaidam Basin (Pullen et al., 2011); and 4. Neogene fluvial sediments (XJ09-003 and XJ09-017) from the Junggar Basin (Yang et al., 2013). These potential sources of eolian dust are located upwind of, or close to, the Altun Red Clay, so they are likely to have provided at least some dust to the Altun deposit.

The spectra for the CHG samples are very similar to that of the Taklamakan samples, with a major age component at 560–400 Ma and a minor age group at 350–200 Ma (Fig. 2a–d). The CHG spectra are also similar to the spectrum of the Qaidam Basin sample (QB), which has a well-defined major peak at c. 450 Ma and a subordinate peak at c. 250 Ma, although the peaks are not as wide, and there is a minor peak at c. 100 Ma that is not present in results for the CHG samples (Fig. 2e). The CHG spectra are different from the Gobi–Alxa arid lands (YG02) and Junggar Basin (XJ09-003 and XJ09-017) spectra, each of which exhibits a major age component at 400–200 Ma and a few ages <200 Ma (Fig. 2f-g) that are not represented in the CHG samples.

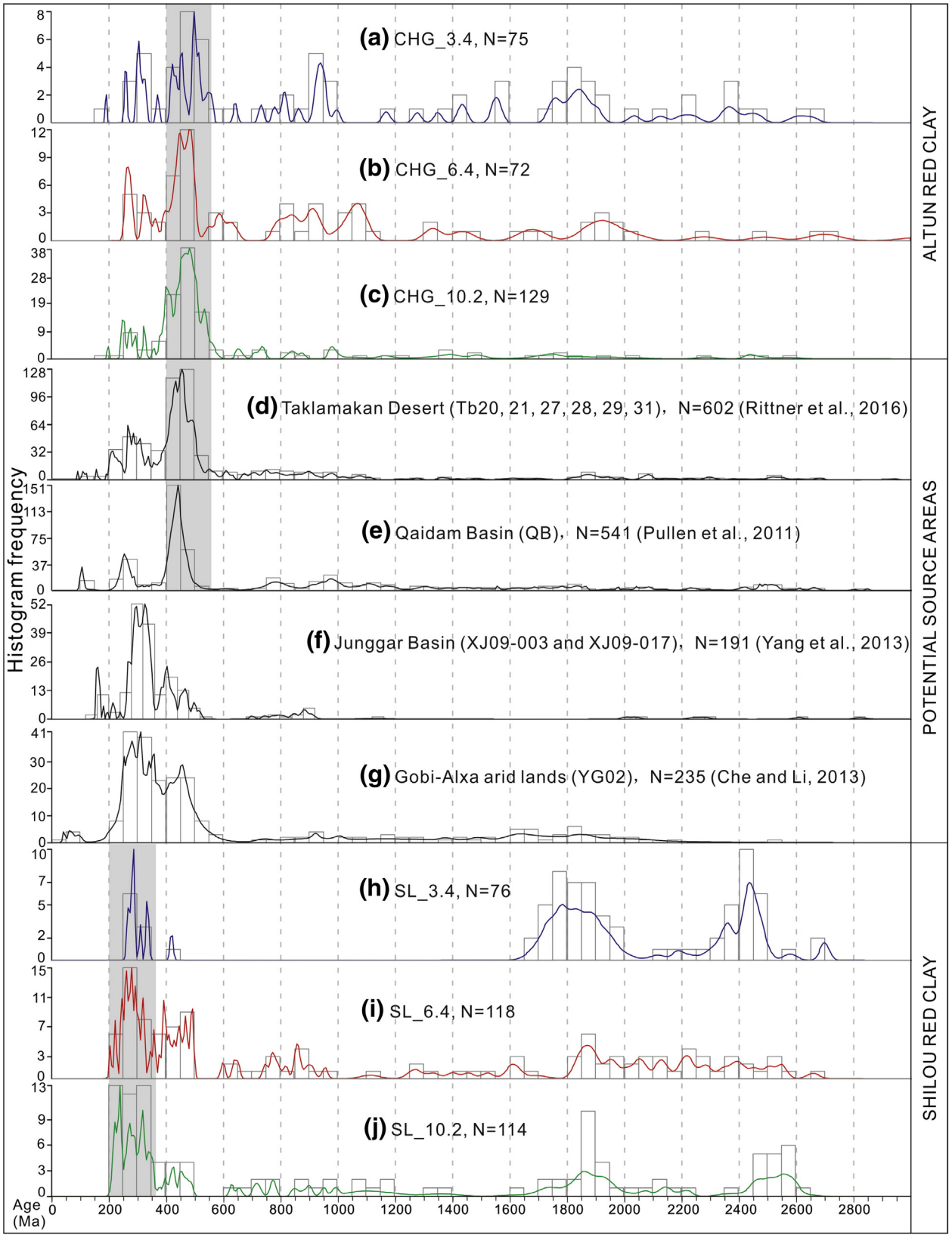

Fig. 2. Comparison of U—Pb detrital zircon ages for the Altun Red Clay (CHG) (a–c), the Shilou Red Clay (SL) (h–j), and potential source areas: Taklamakan Desert, Quidam Basin (QB), Junggar Basin, and Gobi-Alxa arid lands (d–g). Shaded bars indicate approximate ranges of dominant age components. N, number of detrital zircon ages.

Four age spectra of potential source area samples are dominated by the ages <600 Ma (Fig. 2), so this range of zircon U—Pb ages most likely represent the material of the source areas. For this reason, we selected <600 Ma zircon U—Pb ages of the red clay samples as well as source area samples for MDS analysis. In the MDS diagram (Fig. 3), zircon data for the three Altun (CHG) samples plot apart from results for the

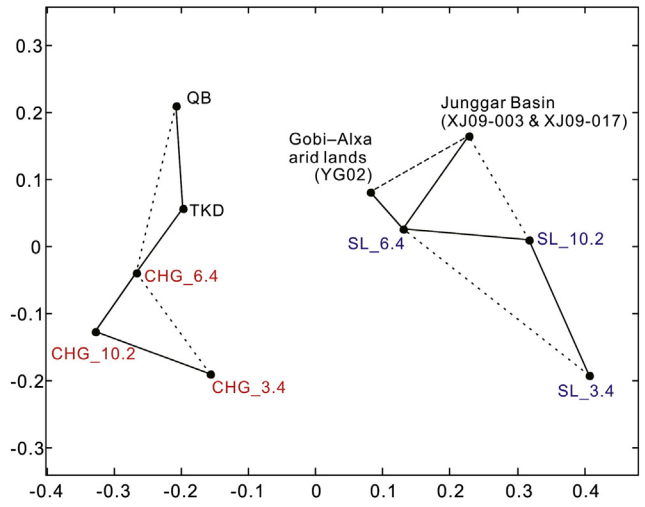

Fig. 3. Metric multidimensional scaling (MDS) plot (Vermeesch, 2013) of detrital zircon age data for the Altun Red Clay (CHG), Shilou Red Clay (SL) and potential source regions: Quidam Basin (QB), Taklimakan Desert (TKD), Junggar Basin, and Gobi-Alxa arid lands. Solid lines and dashed lines connect samples with the closest and second closest neighbors respectively.

Shilou (SL) and Junggar Basin and Gobi–Alxa arid lands samples, but plot close to results obtained from the Taklamakan and Qaidam Basin samples. The Shilou (SL) data are close to those of the Junggar Basin and Gobi–Alxa arid lands.

4. Discussion

4.1. Potential sources of the Altun Red Clay

The detrital zircon age spectra (Fig. 2) and the quantitative MDS map (Fig. 3) both indicate a high degree of similarity between the three Altun Red Clay samples. Furthermore, the mean zircon grain sizes of the three CHG_samples (81 × 52 μm for CHG_3.4, 72 × 49 μm for CHG_6.4, 71 × 45 μm for CHG_10.2) are quite similar to each other. This similarity, over the range of depositional ages from 10.2 to 3.4 Ma, indicates that the sources of dust were stable for at least 7 Ma.

The Altun Red Clay results are also very similar to those for the Taklamakan Desert sample, suggesting that the Taklamakan Desert was a major source area for the Altun Red Clay. There is climatic and geological evidence that the Taklamakan Desert had been established since at least the early Neogene and would have been a viable source of dust. Firstly, the uplifted Tibetan Plateau was sufficiently high and extensive to block southerly-sourced moisture since at least the early Eocene, which triggered the development of aridity in central Asia (Caves et al., 2015; Graham et al., 2005). Retreat of the Paratethys Sea at c. 37 Ma also contributed significantly to Asian interior aridity (Bosboom et al., 2011, 2014; Caves et al., 2015; Zhang et al., 2007). Influenced by these factors (especially by uplift of the Tibetan Plateau), the Tarim Basin was already extremely dry during the Neogene, leading to development of the Taklamakan Desert (Caves et al., 2015; Graham et al., 2005). A recent study has placed inception of the Taklamakan Desert between 26.7 and 22.6 Ma (Zheng et al., 2015). Secondly, the westerly winds that commenced in the early Miocene (Sun et al., 2010), and which continue in the present day (Fig. 1a) (Chen et al., 2008), have had sufficient energy to transport dust from the Taklamakan Desert to Altun Shan. Thirdly, according to the growth model of the Tibetan Plateau, the Altun Shan and surrounding areas were still at relatively low elevations in the Neogene (An et al., 2006; Mulch and Chamberlain, 2006; Wang et al., 2008), which would have facilitated the transportation of dust to the Altun Shan.

Although the MDS diagram (Fig. 3) suggests that the Qaidam Basin results are similar to those for the Altun Red Clay samples, the age spectra show some important differences. The Qaidam Basin spectrum is dominated by a single age component at c. 450 Ma, whereas the Altun Red Clay results indicate a wider age range of 560–400 Ma. The Qaidam spectrum also shows a young component at c. 100 Ma, which is not represented in the Altun data.

The relative proximity of the Qaidam Basin and the Altun Shan suggests that the basin should be considered as a possible source of dust for the Altun Red Clay. The northeastern Qaidam Basin was dominated by lacustrine deposition between about 10 and 6 Ma, with a decrease in lake area around 8 to 6.5 Ma indicated by increased sediment grain size (Fang et al., 2007). Isotope and fossil evidence also indicates that the Qaidam Basin experienced several short dry intervals during which lake areas diminished (Jia et al., 2012; Rea et al., 1998; Chang et al., 2008). Desiccated lacustrine sediments exposed during low lake levels could have contributed dust for eolian deposits (Kapp et al., 2011; Pullen et al., 2011). During dry intervals at c. 8 Ma, the Qaidam Basin was covered by sand, and may have been a dust source for red clay deposited at this time on the CLP; this has been confirmed by detrital zircon provenance studies (Pullen et al., 2011; Nie et al., 2014).

However, we propose that the Qaidam Basin was not a source of dust for the Altun Red Clay, for the following reasons. Firstly, as noted above, the similarity in results for the Altun Red Clay samples of different ages indicates that it had long-term and continuous dust sources. Despite the dry events, the Qaidam Basin was mainly controlled by near-continuous lacustrine deposition during the Neogene (Fang et al., 2007), and therefore is unlikely to have acted as a long-term and continuous source of dust. Secondly, the prevailing winds in the Qaidam Basin are northwesterly, and the Qaidam Basin is downwind of the Xorhol Basin, and so dust entrained from the Qaidam Basin may not have contributed to the Altun Red Clay. Thirdly, the southern Qaidam Basin is bounded by high mountains (elevation >4000 m asl) of the southern Altun Shan, and thermochronology studies indicate that this range was uplifted rapidly between about 14 and 9 Ma (Chen et al., 2002; Jolivet et al., 2001; Wang et al., 2003). Therefore, dust derived from the Qaidam Basin could not have been easily transported out of the basin and to the Xorhol region.

4.2. The wind regime during deposition of the Altun Red Clay

Eastern and western China have been dominated by different climate patterns, westerly winds and monsoons, respectively, since at least the Miocene (Chen et al., 2008; Guo et al., 2002; Miao et al., 2004; Qiang et al., 2011; Sun et al., 2010). Different source areas and wind regimes contributed dust to the eolian red clay deposits in eastern and western China. Although the material composition of the eastern and western red clays is quite similar, clear differences in isotopic characteristics (Sr and Nd isotope results clearly show that the Junggar eolian deposits and those of the CLP define two distinct groups) reflect different dust sources (Sun, 2002; Sun et al., 2010).

However, which climate pattern, westerly winds or monsoons (or both), had the most influence on deposition of the Altun Red Clay? To investigate, we compare the detrital zircon ages (especially the main component) of the Altun Red Clay with those for the Shilou Red Clay sequence of the eastern CLP, using coeval samples from the two sections, with depositional ages of 10.2, 6.4, and 3.4 Ma.

Both the age spectra (Fig. 2) and the MDS diagram (Fig. 3) show clear differences between the Altun Red Clay and the Shilou Red Clay samples. The three Altun samples share a uniform age distribution at 560–400 Ma, whereas the Shilou samples are dominated by components at 360–200 Ma, and minor components at 500–400 Ma (Fig. 2). Sample SL_3.4 sample also shows significant peaks of Paleoproterozoic age (2000–1700 Ma and 2600–2300 Ma). Zircons of these ages are present in sediment samples from the middle reaches of the Yellow River (Nie et al., 2015) as well as in basement rock samples of the Lüliang Shan (Liu et al., 2011; Zhao et al., 2008). In addition, the mean zircon grain size in sample SL_3.4 (114 × 67 μm) is greater than in sample SL_6.4 (58 × 37 μm) and SL_10.2 sample (59 × 37 μm). Considering that the

Shilou Red Clay section is flanked to the east by the Lüliang Shan, and is close to the middle reaches of the Yellow River, the Shilou Red Clay may contain a detrital contribution from the nearby exhumed Lüliang Shan or Yellow River sediments since late Pliocene (although which source may be dominant needs further study). However, the similarity of age spectra (Fig. 2) and the MDS diagram (Fig. 3) indicate a close relationship between the Shilou Red Clay samples and Junggar Basin and Gobi–Alxa arid lands samples, which suggests that the desert and arid lands of northwestern China likely served as major source areas for the Shilou Red Clay.

These observations indicate that the Altun and Shilou Red Clays were likely derived from distinct source areas and transported by different wind systems. If the eolian red clay deposits of the CLP were mainly derived from the desert and Gobi areas of northwest China, transport was most likely by the East Asian winter monsoon (Lu et al., 2001; Miao et al., 2004; Sun et al., 2010), whereas we have demonstrated that the dust of the Altun Red Clay was most likely transported by the westerly wind regime from the Taklimakan Desert.

Furthermore, if the Xorhol area was dominated by monsoon winds, then the dust in the Altun Red Clay would be expected to have originated in the Gobi–Alxa arid lands and Junggar Basin, which are located upwind of the Altun Red Clay. However, our detrital zircon results do not support these areas as the main sources for the Altun Red Clay, hence the East Asian winter monsoon is unlikely to have been the dominant transportation agent of dust to the Altun Red Clay. In addition, Li et al. (2014) suggested, based on pronounced differences in magnetic susceptibility between the Altun Red Clay and the CLP deposits, that the summer monsoon was unable to affect Altun Shan due to blocking by the uplifted Tibetan Plateau. In summary, we propose that the dust of the Altun Red Clay was transported by westerly winds and not by the East Asian monsoon.

5. Conclusions

The detrital zircon age spectra of Altun Red Clay samples, deposited at 10.2, 6.4, and 3.4 Ma are very similar, suggesting long-term, stable major dust sources. Based on the age spectra and quantitative MDS analysis, together with climatic and geological evidence, we conclude that the Taklamakan Desert served as the main source region for the Altun Red Clay. However, the possibility that other provenance areas provided eolian materials to the Altun Red Clay cannot entirely be excluded.

The detrital zircon age spectra of Altun Red Clay samples are quite different from those of the coeval Shilou Red Clay (SL) samples from eastern CLP, suggesting that the Altun and Shilou Red Clays were sourced from different areas, and the material transport was controlled by different wind regimes. We suggest that the dust in the Altun Red Clay was transported mainly via westerly winds.

Acknowledgments

The authors are grateful to Qingsong Liu for making valuable and insightful comments that considerably improved the manuscript, to Xiaolong Zhou for field assistance, and to Shuangshuang Wang for laboratory assistance. MTDW publishes with permission of the Executive Director of the Geological Survey of Western Australia. This study was supported by the National Natural Science Foundation of China (Grant Nos. 41502174, 41002052, 41202133), and Nonprofit Special Project of Land Resources (Grant No. 201311126).

Appendix A. Supplementary data

Supplementary data to this article can be found online at http://dx.doi.org/10.1016/j.palaeo.2016.07.020.

References

An, Z.S., Sun, D.H., Chen, M.Y., Sun, Y.B., Li, L., Chen, B.Q., 2000. Red clay sequences in Chinese Loess Plateau and recorded paleoclimate events of the late Tertiary. Quat. Sci. 5 (5), 435–446 (in Chinese).

An, Z.S., Zhang, P.Z., Wang, E.Q., Wang, S.M., Qiang, X.K., Li, L., Song, Y.G., Chang, H., Liu, X.D., Zhou, W.J., Liu, W.G., Cao, J.J., Li, X.Q., Shen, J., Liu, Y., Ai, L., 2006. Changes of the monsoon-arid environment in China and growth of the Tibetan plateau since the Miocene. Quat. Sci. 26 (5), 678–693 (in Chinese).

Bosboom, R.E., Dupont-Nivet, G., Houben, A.J.P., Brinkhuis, H., Villa, G., Mandic, O., Stoica, M., Zachariasse, W.J., Guo, Z.J., Li, C.X., Krijgsman, W., 2011. Late Eocene sea retreat from the Tarim Basin (west China) and concomitant Asian paleoenvironmental change. Palaeogeogr. Palaeoclimatol. Palaeoecol. 299, 385–398.

Bosboom, R.E., Abels, H.A., Hoorn, C., Berg, B.C.J., Guo, Z., Dupont-Nivet, G., 2014. Aridification in continental Asia after the Middle Eocene Climatic Optimum (MECO). Earth Planet. Sci. Lett. 389, 34–42.

Caves, J.K., Winnick, M.J., Graham, S.A., Sjostrom, D.j., Mulch, A., Chamberlain, C.P., 2015. Role of the westerlies in Central Asia climate over the Cenozoic. Earth Planet. Sci. Lett. 428, 33–43.

Chang, M.M., Wang, X.M., Liu, H.Z., Miao, D.S., Zhao, Q.H., Wu, G.X., Liu, J., Li, Q., Sun, Z.C., Wang, N., 2008. Extraordinarily thick-boned fish linked to the aridification of the Qaidam Basin (northern Tibetan Plateau). Proc. Natl. Acad. Sci. U. S. A. 105, 13246–13251.

Che, X.D., Li, G.J., 2013. Binary sources of loess on the Chinese Loess Plateau revealed by U—Pb ages of zircon. Quat. Res. 80 (3), 545–551.

Chen, Z.L., Wan, J.L., Chen, X.H., Pan, J.H., 2002. Rapid strike-slip of the Altyn Tagh Fault at 8 Ma and its geological implications. Acta Geosci. Sin. 23 (4), 295–300 (in Chinese with English abstract).

Chen, J., Li, G.J., Yang, J.D., Rao, W.B., Lu, H.Y., Balsam, W., Sun, Y.B., Ji, J.F., 2007. Nd and Sr isotopic characteristics of Chinese deserts: implications for the provenances of Asian dust. Geochim. Cosmochim. Acta 71 (15), 3904–3914.

Chen, F.H., Yu, Z.C., Yang, M.L., Ito, E., Wang, S.M., Madsen, D.B., Huang, X.Z., Zhao, Y., Sato, T., John, B., Birks, H., Boomer, I., Chen, J.H., An, C.B., Wünnemann, B., 2008. Holocene moisture evolution in arid central Asia and its out-of-phase relationship with Asian monsoon history. Quat. Sci. Rev. 27 (3–4), 351–364.

Derbyshire, E., Meng, X., Kemp, R.A., 1998. Provenance, transport and characteristics of modern aeolian dust in western Gansu Province, China, and interpretation of the Quaternary loess record. J. Arid Environ. 39 (3), 497–516.

Ding, Z.L., Sun, J.M., Yang, S.L., Liu, T.S., 2001. Geochemistry of the Pliocene red clay formation in the Chinese Loess Plateau and implications for its origin, source provenance and paleoclimate change. Geochim. Cosmochim. Acta 65, 901–913.

Fang, X.M., Zhang, W.L., Meng, Q.Q., Gao, J.P., Wang, X.M., King, J., Song, C.H., Dai, S., Miao, Y.F., 2007. High-resolution magnetostratigraphy of the Neogene Huaitoutala section in the eastern Qaidam Basin on the NE Tibetan Plateau, Qinghai Province, China and its implication on tectonic uplift of the NE Tibetan Plateau. Earth Planet. Sci. Lett. 258 (1–2), 293–306.

Graham, S.A., Chamberlain, C.P., Yue, Y.J., Ritts, B.D., Hanson, A.D., Horton, T.W., Waldbauer, J.R., Poage, M.A., Feng, X., 2005. Stable isotope records of Cenozoic climate and topography, Tibetan plateau and Tarim basin. Am. J. Sci. 305, 101–118.

Guo, Z.T., Peng, S.Z., Hao, Q.Z., Biscaye, P.E., Liu, T.S., 2001. Origin of the Miocene–Pliocene Red-Earth Formation at Xifeng in Northern China and implications for paleoenvironments. Palaeogeogr. Palaeoclimatol. Palaeoecol. 170 (1), 11–26.

Guo, Z.T., Ruddiman, W.F., Hao, Q.Z., Wu, H.B., Qiao, Y.S., Zhu, R.X., Peng, S.Z., Wei, J.J., Yuan, B.Y., Liu, T.S., 2002. Onset of Asian desertification by 22 Myr ago inferred from loess deposits in China. Nature 416 (6877), 159–163.

Jahn, B.M., Gallet, S., Han, J.M., 2001. Geochemistry of the Xining, Xifeng and Jixian sections, Loess Plateau of China: eolian dust provenance and paleosol evolution during the last 140 ka. Chem. Geol. 178 (1), 71–94.

Jia, G., Li, Z., Peng, P.A., Zhou, L., 2012. Aeolian n-alkane isotopic evidence from North Pacific for a Late Miocene decline of C_4 plant in the arid Asian interior. Earth Planet. Sci. Lett. 321–322, 32–40.

Jolivet, M., Brunel, M., Seward, D., Xu, Z., Yang, J., Roger, F., Tapponnier, P., Malavieille, J., Arnaud, N., Wu, C., 2001. Mesozoic and Cenozoic tectonics of the northern edge of the Tibetan plateau: fission–track constraints. Tectonophysics 343 (1), 111–134.

Kapp, P., Pelletier, J.D., Rohrmann, A., Heermance, R., Russell, J., Ding, L., 2011. Wind erosion in the Qaidam basin, central Asia: implications for tectonics, paleoclimate, and the source of the Loess plateau. GSA Today 21 (4), 4–10. http://dx.doi.org/10.1130/GSATG99A.1.

Li, G.J., Chen, J., Ji, J.F., Yang, J.D., Conway, T.M., 2009. Natural and anthropogenic sources of East Asian dust. Geology 37 (8), 727–730.

Li, J.X., Yue, L.P., Pan, F., Zhang, R., Guo, L., Xi, R.G., Guo, L., 2014. Intensified aridity of the Asian interior recorded by the magnetism of red clay in Altun Shan, NE Tibetan Plateau. Palaeogeogr. Palaeoclimatol. Palaeoecol. 411 (0), 30–41.

Liu, T.S., 1985. Loess and the Environment. China Ocean Press, Beijing.

Liu, C.Q., Masuda, A., Okada, A., Yabuki, S., Fan, Z.L., 1994. Isotope geochemistry of Quaternary deposits from the arid lands in northern China. Earth Planet. Sci. Lett. 127 (1–4), 25–38.

Liu, C., Zhao, G., Sun, M., Wu, F., Yang, J., Yin, C., et al., 2011. U—Pb and Hf isotopic study of detrital zircons from the Yejishan Group of the Lüliang Complex: constraints on the timing of collision between the Eastern and Western Blocks, North China Craton. Sediment. Geol. 236 (1–2), 129–140.

Lu, Y.C., Wen, Q.Z., Huang, B.J., Min, Y.S., Deng, H.X., 1976. A preliminary discussion on the source of loess materials in China—a study of the surface textures of silt quartz grains by transmission electron microscope. Geochimica (01), 47–53 (in Chinese).

Lu, H.Y., Vandenberghe, J., An, Z.S., 2001. Aeolian origin and palaeoclimatic implications of the 'red clay' (north China) as evidenced by grain–size distribution. J. Quat. Sci. 16 (1), 89–97.

Maher, B.A., Mutch, T.J., Cunningham, D., 2009. Magnetic and geochemical characteristics of Gobi Desert surface sediments: implications for provenance of the Chinese Loess Plateau. Geology 37, 279–282. http://dx.doi.org/10.1130/G25293A.1.

Miao, X.D., Sun, Y.B., Lu, H.Y., Mason, J.A., 2004. Spatial pattern of grain size in the Late Pliocene 'Red Clay' deposits (North China) indicates transport by low-level northerly winds. Palaeogeogr. Palaeoclimatol. Palaeoecol. 206 (1–2), 149–155.

Mulch, A., Chamberlain, C.P., 2006. The rise and growth of Tibet. Nature 439 (7077), 670–671.

Nie, J.S., Peng, W.B., Möller, A., Song, Y.G., Stockli, D.F., Stevens, T., Horton, B.K., Liu, S.P., Bird, A., Oalmann, J., Gong, H.J., Fang, X.M., 2014. Provenance of the upper Miocene–Pliocene Red Clay deposits of the Chinese loess plateau. Earth Planet. Sci. Lett. 407 (0), 35–47.

Nie, J., Stevens, T., Rittner, M., Stockli, D., Garzanti, E., Limonta, M., et al., 2015. Loess Plateau storage of Northeastern Tibetan Plateau-derived Yellow River sediment. Nat. Commun. 6, 8511.

Pullen, A., Kapp, P., McCallister, A.T., Chang, H., Gehrels, G.E., Garzione, C.N., Heermance, R.V., Ding, L., 2011. Qaidam Basin and northern Tibetan Plateau as dust sources for the Chinese Loess Plateau and paleoclimatic implications. Geology 39 (11), 1031–1034.

Qiang, X.K., An, Z.S., Song, Y.G., Chang, H., Sun, Y.B., Liu, W., Ao, H., Dong, J.B., Fu, C.F., Wu, F., Lu, F.Y., Cai, Y.J., Zhou, W.J., Cao, J.J., Xu, X.W., Ai, L., 2011. New eolian red clay sequence on the western Chinese Loess Plateau linked to onset of Asian desertification about 25 Ma ago. Sci. China Earth Sci. 54 (1), 136–144.

Rea, D.K., Snoeckx, H., Joseph, L.H., 1998. Late Cenozoic Eolian deposition in the North Pacific: Asian drying, Tibetan uplift, and cooling of the northern hemisphere. Paleoceanography 13 (3), 215–224.

Rittner, M., Vermeesch, P., Carter, A., Bird, A., Stevens, T., Garzanti, E., et al., 2016. The provenance of Taklamakan desert sand. Earth Planet. Sci. Lett. 437, 127–137.

Shang, Y., Beets, C.J., Tang, H., Prins, M.A., Lahaye, Y., van Elsas, R., et al., 2016. Variations in the provenance of the late Neogene Red Clay deposits in northern China. Earth Planet. Sci. Lett. 439, 88–100.

Stevens, T., Palk, C., Carter, A., Lu, H., Clift, P.D., 2010. Assessing the provenance of loess and desert sediments in northern China using U—Pb dating and morphology of detrital zircons. Geol. Soc. Am. Bull. 122 (7–8), 1331–1344.

Stevens, T., Carter, A., Watson, T.P., Vermeesch, P., Andò, S., Bird, A.F., Lu, H., Garzanti, E., Cottam, M.A., Sevastjanova, I., 2013. Genetic linkage between the Yellow River, the Mu Us desert and the Chinese Loess Plateau. Quat. Sci. Rev. 78 (0), 355–368.

Sun, J.M., 2002. Provenance of loess material and formation of loess deposits on the Chinese Loess Plateau. Earth Planet. Sci. Lett. 203 (3–4), 845–859.

Sun, J.M., Windley, B.F., 2015. Onset of aridification by 34 Ma across the Eocene-Oligocene transition in Central Asia. Geology 11 (43), 1015–1018.

Sun, J.M., Zhang, M.Y., Liu, T.S., 2001. Spatial and temporal characteristics of dust storms in China and its surrounding regions, 1960–1999: relations to source area and climate. J. Geophys. Res. 106 (D10), 10325–10333.

Sun, Y.B., Tada, R., Chen, J., Liu, Q.S., Toyoda, S., Tani, A., Ji, J.F., Isozaki, Y., 2008. Tracing the provenance of fine-grained dust deposited on the central Chinese Loess Plateau. Geophys. Res. Lett. 35 (1), 244–259.

Sun, J.M., Ye, J., Wu, W.Y., Ni, X.J., Bi, S.D., Zhang, Z.Q., Liu, W.M., Meng, J., 2010. Late Oligocene-Miocene mid-latitude aridification and wind patterns in the Asian interior. Geology 38 (3–4), 515–518.

Újvári, G., Klötzli, U., 2015. U—Pb ages and Hf isotopic composition of zircons in Austrian last glacial loess: constraints on heavy mineral sources and sediment transport pathways. Int. J. Earth Sci. 104 (5), 1365–1385.

Újvári, G., Klötzli, U., Kiraly, F., Ntaflos, T., 2013. Towards identifying the origin of metamorphic components in Austrian loess: insights from detrital rutile chemistry, thermometry and U–Pb geochronology. Quat. Sci. Rev. 75 (0), 132–142.

Van Achterbergh, E., Ryan, C.G., Jackson, S.E., Griffin, W.L., 2001. Data reduction software for LA-ICP-MS. In: Sylvester, P.J. (Ed.), Laser-ablation-ICPMS in the Earth Sciences. Principles and Applications. Mineralogical Society of Canada Short Course Series 29, pp. 239–243.

Vermeesch, P., 2013. Multi-sample comparison of detrital age distributions. Chem. Geol. 341, 140–146.

Wang, E., Wan, J.L., Liu, J.Q., 2003. Late Cenozoic geological evolution of the foreland basin bordering the West Kunlun range in Pulu area: constraints on timing of uplift of northern margin of the Tibetan Plateau. J. Geophys. Res. 108 (B8).

Wang, X.M., Dong, Z.B., Zhang, J.W., Liu, L.C., 2004. Modern dust storms in China: an overview. J. Arid Environ. 58 (4), 559–574.

Wang, C.S., Zhao, X.X., Liu, Z.F., Lippert, P.C., Graham, S.A., Coe, R.S., Yi, H.S., Zhu, L.D., Liu, S., Li, Y.L., 2008. Constrains on the early uplift history of the Tibetan plateau. Proc. Natl. Acad. Sci. U. S. A. 105 (13), 4987–4992.

Whalley, W.B., Marshall, J.R., Smith, B.J., 1982. Origin of desert loess from some experimental observations. Nature 300 (5891), 433–435.

Wiedenbeck, M., Hanchar, J.M., Peck, W.H., Sylvester, P., Valley, J., Whitehouse, M., Kronz, A., Morishita, Y., Nasdala, L., Fiebig, J., Franchi, I., Girard, J.-P., Greenwood, R.C., Hinton, R., Kita, N., Mason, P.R.D., Norman, M., Ogasawara, M., Piccoli, P.M., Rhede, D., Satoh, H., Schulz-Dobrick, B., Skår, O., Spicuzza, M.J., Terada, K., Tindle, A., Togashi, S., Vennemann, T., Xie, Q., Zheng, Y.F., 2004. Further characterisation of the 91500 zircon crystal. Geostand. Geoanal. Res. 28, 9–39.

Wu, G., Zhang, C., Zhang, X., Tian, L., Yao, T., 2010. Sr and Nd isotopic composition of dust in Dunde ice core, northern China: implications for source tracing and use as an analogue of long-range transported Asian dust. Earth Planet. Sci. Lett. 299, 409–416. http://dx.doi.org/10.1016/j.epsl.2010.09.021.

Xiao, G.Q., Zong, K.Q., Li, G.J., Hu, Z.C., Dupont Nivet, G., Peng, S.Z., Zhang, K.X., 2012. Spatial and glacial–interglacial variations in provenance of the Chinese Loess Plateau. Geophys. Res. Lett. 39 (20), L20715.

Xu, Y., Yue, L.P., Li, J.X., Sun, L., Sun, B., Zhang, J.Y., Ma, J., Wang, J.Q., 2009. An 11-Ma–old red clay sequence on the Eastern Chinese Loess Plateau. Palaeogeogr. Palaeoclimatol. Palaeoecol. 284 (3–4), 383–391.

Yang, W., Jolivet, M., Dupont-Nivet, G., Guo, Z.J., Zhang, Z.C., Wu, C.D., 2013. Source to sink relations between the Tian Shan and Junggar Basin (northwest China) from Late Palaeozoic to Quaternary: evidence from detrital U–Pb zircon geochronology. Basin Res. 25, 219–240.

Yue, L.P., 1995. Palaeomagnetic polarity boundary were recorded in Chinese loess and red clay, and geological significance. Acta Geophys. Sin. 38 (3), 310–320 (in Chinese).

Zhang, Z.S., Wang, H.J., Guo, Z.T., Jiang, D.B., 2007. What triggers the transition of palaeoenvironmental patterns in China, the Tibetan Plateau uplift or the Paratethys Sea retreat? Palaeogeogr. Palaeoclimatol. Palaeoecol. 245, 317–331.

Zhao, G., Wilde, S.A., Sun, M., Li, S., Li, X., Zhang, J., 2008. SHRIMP U–Pb zircon ages of granitoid rocks in the Lüliang Complex: implications for the accretion and evolution of the Trans-North China Orogen. Precambrian Res. 160 (3–4), 213–226.

Zheng, H.B., Wei, X.C., Tada, R., Clift, P.D., Wang, B., Jourdan, F., Wang, P., He, M.Y., 2015. Late Oligocene–early Miocene birth of the Taklimakan Desert. Proc. Natl. Acad. Sci. U. S. A. 112 (25).